Journal of Power Sources 195 (2010) 2795–2799

Contents lists available at ScienceDirect

Journal of Power Sources

journal homepage: www.elsevier.com/locate/jpowsour

Direct observation of the two-phase flow in the air channel of a proton exchange membrane fuel cell and of the effects of a clogging/unclogging sequence on the current density distribution

Jerome Dillet[a,*], Olivier Lottin[a], Gael Maranzana[a], Sophie Didierjean[a], Delphine Conteau[a,b], Caroline Bonnet[b]

[a] LEMTA, CNRS, Nancy University, avenue de la Fort de Haye, 54500 Vandoeuvre les Nancy, France
[b] LSGC, CNRS, Nancy University, rue Grandville, 54000 Nancy, France

ARTICLE INFO

Article history:
Received 3 July 2009
Received in revised form
24 September 2009
Accepted 21 October 2009
Available online 13 November 2009

Keywords:
PEM fuel cells
Instrumented cell
Water visualisation
Current density profile
Cathode channel flooding

ABSTRACT

A small single-channel fuel cell prototype was built with the objective of monitoring the appearance and transport of water droplets in the gas channels in usual operating conditions. It allows the simultaneous observation of droplets and of their local effects on current density. The first results show that the air flow rate seems to control the transition between two different water removal mechanisms: a plug flow when the air stoichiometry is low, with significant disturbances in the local current density, pressure drop and fuel cell performance, and a more conventional flow with steadier removal of smaller droplets when the stoichiometry is higher.

1. Introduction

Bipolar plates are key components of PEM fuel cells (PEMFC) because of their multiple functions: they allow the distribution of gases to the reaction sites and the collection of the electric current. In addition, they ensure the evacuation of the heat and water produced by the reaction. The performances of a PEMFC are strongly dependent on the transport processes occurring within the bipolar plate gas channels. Water management is one of the critical issues for the optimisation of PEMFC: on one hand, the membrane must be hydrated to allow the transport of protons from the anode side to the cathode side. On the other hand, an excess of water can be detrimental to the efficiency of the fuel cell: liquid water may hinder the transport of oxygen through the porous structure of the gas diffusion layer (GDL) toward the catalyst layer, or it can lead to the formation of water columns inside the gas channels, thus preventing or restraining the flow of oxygen or hydrogen downstream. As direct consequences, the performance of the cell decreases and the total pressure drop increases [1,2].

In order to facilitate the investigation of mass, charge and heat transfer phenomena occurring in PEM fuel cells, various research groups built prototypes in which the bipolar plates are replaced by transparent plates, which allows the observation of water condensation and flow. Mench et al. [3] use a single-channel fuel cell with segmented current collection at the cathode. They studied the evolution of non-uniformities in the current density as function of the operating conditions (from drying to flooding). Maranzana et al. [4] and Hakenjos et al. [5] also used local current collection but with parallel channels flow field plates. Temperature measurements with thermocouples, or by infrared thermometry, show a strong correlation with the local current density. Su et al. [6], Weng et al. [7], Ous and Arcoumanis [8], Shanhai and Wang [2] and Yang et al. [9] attempted to localise liquid water in the gas channels thanks to cameras or video cameras but mostly in stationary regime. Pictures of the channel [9] show the appearance of droplets on the GDL surface. These images and pressure drop measurements [2] provide information about the effect of the hydrophobicity of the GDL on water condensation and transport. Other authors [4,5,7] report about the presence of a liquid front (before which no liquid water can be observed) in parallel channels.

Su et al. [6] exploited their results in optimising the channels design by minimizing liquid retention. Other more delicate techniques which require also heavier equipments can provide

* Corresponding author.
E-mail address: jerome.dillet@ensem.inpl-nancy.fr (J. Dillet).

0378-7753/$ – see front matter © 2009 Elsevier B.V. All rights reserved.
doi:10.1016/j.jpowsour.2009.10.103

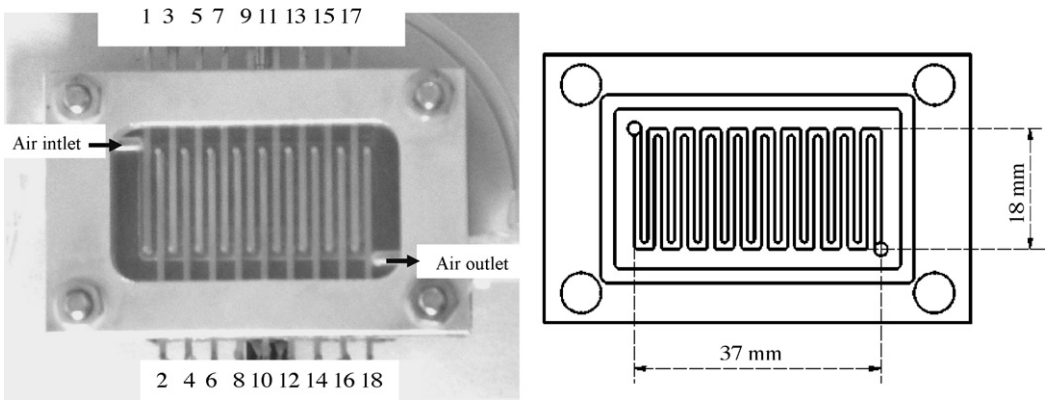

Fig. 1. Prototype of the single-channel fuel cell; the golded brass strips are numbered from 1 to 18 (left). Sketch of the gas channels of 0.7 mm×1 mm cross-section (right).

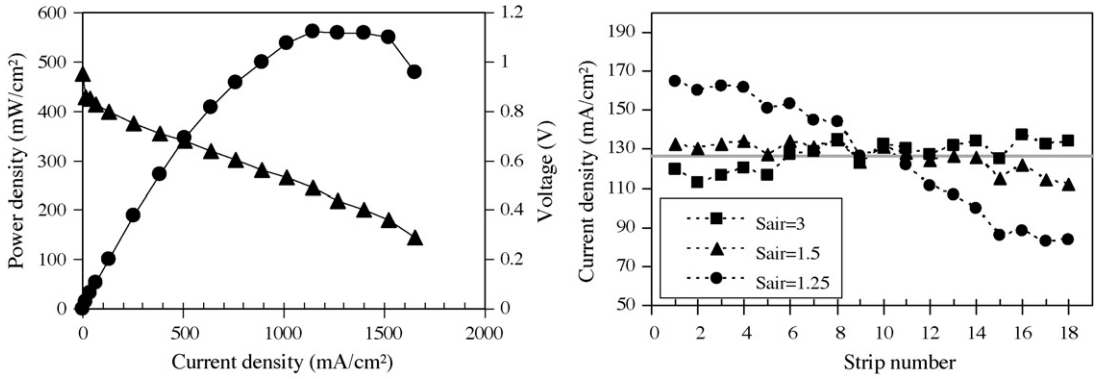

Fig. 2. (left) Fuel cell voltage and power density vs. current density (▲ voltage; ●, power density) and (right) current density profile as a function of the air stoichiometry. The horizontal line represents the average current density and the total current intensity is set to 1 A.

information about liquid water in fuel cells: Hartnig et al. [10] built live images of droplets formation using X-ray tomography whereas Bedet et al. [11] used nuclear magnetic resonance imaging. In all of these works, the main objective remains the optimisation of water management in PEM fuel cells and more generally, of the fluid flows.

The manuscript is divided into two sections; the single-channel fuel cell prototype is presented in the first section while in the second part we report the observation of clogging/unclogging sequences in the air channel.

2. Experimental setup

2.1. Segmented fuel cell

The segmented fuel cell (Fig. 1) consists of a plate of golded aluminium (at the anode), and of a transparent PMMA plate equipped with 18 golded brass current collectors (at the cathode). The hydrogen channel is machined in the anodic plate whereas the brass strips inserted into the PMMA plate delimit the air channel. The pressure drop in the air channel is quite important: it varies quasi-linearly between 0 and 150 mbar with the airflow (from 0 to 40 SLPH (standard liters per hour)).

The fuel cell temperature is controlled thanks to an electric heating system fixed on the anodic plate. Nevertheless, significant thermal gradients exist probably within the cell because of the thermal resistances of the various components and of their interfaces. Mass flow controllers are used for both gases and the air is humidified up to about 80% RH thanks to a bubbler. The air RH is assumed equal to the vapour saturation ratio at the temperatures of the fuel cell and of the bubbler, given by Rankine' formula: $P_{sat} = P_0 \exp(13.7 - 5096/T(K))$, with P_0 the standard pressure.

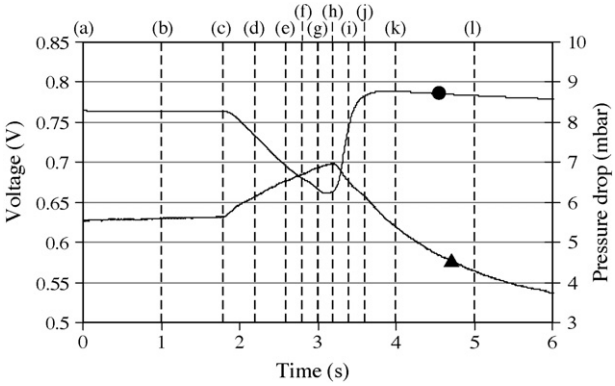

Fig. 3. Voltage (●) and pressure drop (▲) vs. time during a clogging/unclogging sequence. Dashed lines correspond to the pictures of Fig. 5.

2.2. Data acquisition and processing

In order to detect the current intensity collected by the 18 brass strips with the least possible perturbations, a passive electronic circuit is used where each of them is connected to a 10 mΩ shunt resistance which voltage drop allows an indirect measurement. A particular attention was given to this circuit in order to reduce and to make as much as possible uniform all parasitic (contact and con-

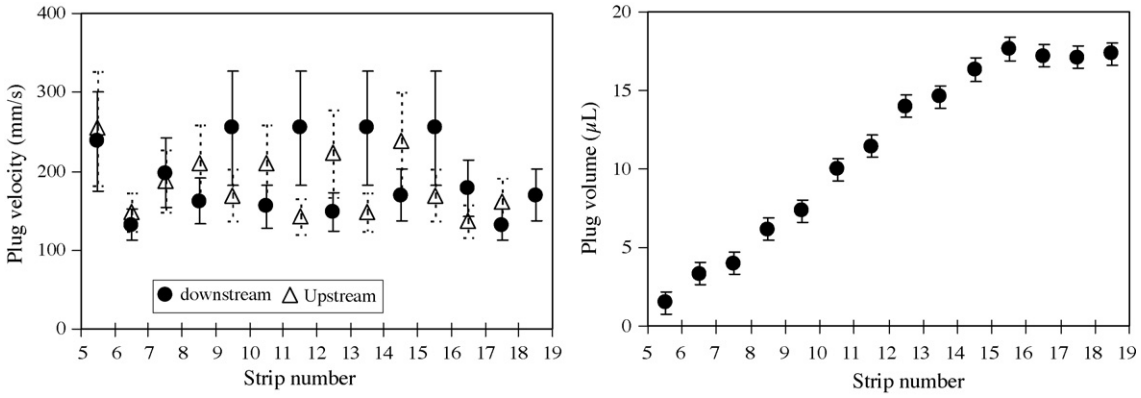

Fig. 4. Plug velocity (left) and vulum (right) along the air channel.

necting) resistances, so that the cathodic gas diffusion layer can be considered as isopotential. The total current intensity is controlled by an Amrel FEL-60-1 electronic load. Numerical data (local current intensities, voltage, pressure drops and temperature) are recorded at a frequency of 200 Hz and with a 16-bit resolution thanks to a National Instrument SCXI multiplexer. A high speed Photron (FASTCAM MS3000APX) camera with an 8 bits 1024×1024 resolution sensor is used for the digital video recording. It allows up to 3000 fps in full resolution. The video frames and the data files are synchronized.

2.3. Fuel cell performances

The MEA (Johnson-Matthey) consists of a 30 μm PFSA polymer membrane and of catalytic layers with an average Pt loading of 0.406 mg cm^{-2} at the anode and 0.385 mg cm^{-2} at the cathode. The active area is $A = 7.9\,\text{cm}^2$. The GDL is a 190 μm thick carbon fibre paper (TorayTM TGP-H-060). Air and hydrogen flow in opposite directions (counter-flow) for a better homogeneity of current densities. The pressure is equal to the atmospheric pressure (except for the losses) and the temperature is close to 52 °C. The brass strips are numbered so that the first one is near the air inlet and the 18th is near the hydrogen inlet. The fuel cell polarisation curve is given in Fig. 2, the measurements being carried out at fixed current with stoichiometries set to $S_{air} = 3$ and $S_{H_2} = 1.4$. The performances are good, with a maximum current density of 1.8–2 A cm^{-2} and a power density reaching 0.55 W cm^{-2}.

The current density profile provides local information about the fuel cell operation through the effects of water distribution: dry or flooded areas yields lower current densities. For instance, Fig. 2 depicts the effect of the air stoichiometry: a decrease in the airflow induces an inclination of the current density profile toward the air exit with a slight decrease in the fuel cell voltage. The current densities are the most uniform when the air stoichiometry is close to 1.5.

3. Clogging/unclogging sequence

Water droplets are more easily observed when the current density and the air stoichiometry are low (in this case, $j = 127\,\text{mA cm}^{-2}$ and $S_{air} = 1.5$). After a few minutes, liquid plugs appear in channel and they are quickly removed by the airflow. The time between two successive clogs varies between 1 and 5 min and generally, they form between the 5th and the 12th strip. Fig. 3 shows the duration of the total clogging/unclogging sequence: the plug is evacuated in 1.5 s. Meanwhile, the pressure drop increases and the fuel cell voltage decreases by about 12%.

The high speed camera allows the direct observation of the plugs (Fig. 5) and makes it possible to estimate their velocity starting from the pictures. In fact, two different values can be obtained depending on which meniscus (front or back) is used as reference. Although a strong dispersion of the results can be observed in Fig. 4, the velocity along the gas channel seems to remain constant in average. The mean value is 190 mm s^{-1}, which is about one-third of the mean velocity of air in the free channel (1.5 SLPH corresponding to 550 mm s^{-1}). This difference can be explained on one hand by the rise in pressure (upstream the plug, including the relatively large volume of the bubbler) and on the other hand by a possible airflow through the gas diffusion layer below the strips. The second graph shows that the volume of the plug increases linearly until the 16th strip, which can be related to an uniform current density along the channel. The volume remains approximately constant starting from the 16th strip, probably because of droplets separation or deposition behind the plug.

Videos illustrating the whole sequence can be found on the Lemta website http://www.lemta.fr/pac.html or following the link given in reference[1]. The synchronization of the frames with the current density profiles provides a good understanding of the coupling between the two-phase flow in the channel and the fuel cell performance (Fig. 5). The major effects are linked with the impoverishment of air downstream the plug. The total current being imposed by the electronic load (1 A), the decrease in current density downstream the plug is compensated by an increase upstream because the sum of the local currents is equal to the set 1 A. Complementary measurements carried out at constant voltage show similar results but since there is no artificial compensation (upstream) of the drop in local current densities (downstream), the overall decrease in electrical power reaches about 37% (instead of 12%).

The influence of the airflow was also investigated. In particular, it was noticed that when the air stoichiometry reached $S_{air} = 3$ (which is equivalent to doubling the air velocity and results in a 12% pressure drop increase) the flow pattern and the fuel cell behaviour are completely different: the pressure drop, the voltage and the current density profile are not any more subjected to strong perturbations. The video recordings show a steady removal of smaller droplets, without formation of plug in the channel. Before being carried away by the airflow, some droplets move slowly along the channel wall. This is illustrated by a video on the website http://www.lemta.fr/pac.html. It can also be accessed directly following the link given in reference[2].

[1] http://perso.ensem.inpl-nancy.fr/Jerome.Dillet/JPSarticle/LowStoichiometryPlug.avi.
[2] http://perso.ensem.inpl-nancy.fr/Jerome.Dillet/JPSarticle/HighStoichiometryPlug.avi.

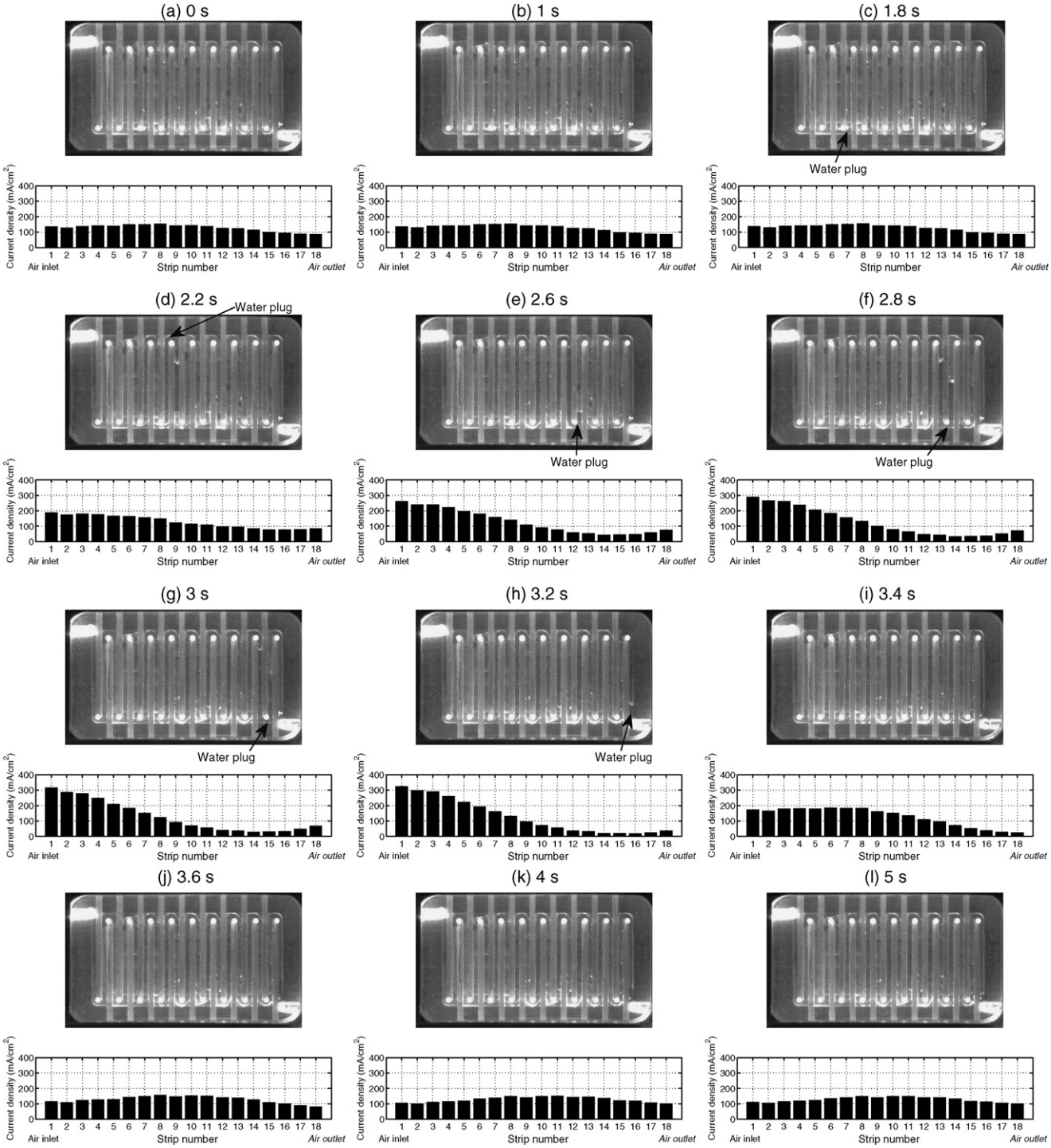

Fig. 5. Formation and evolution of a plug in the air channel and corresponding local current densities (at fixed total current intensity 1 A).

4. Conclusion and perspectives

The air flow rate seems to control the transition between two different water removal mechanisms: a plug flow when the air stoichiometry is low, with significant disturbances in the local current density, pressure drop and fuel cell performance, and a more conventional flow with steadier removal of smaller droplets when the stoichiometry is higher. Future works will focus on the understanding of the transition between these flow patterns as a function of the fuel cell operating conditions and of the channel geometry. Comparison with usual two-phase flow pattern maps will help to investigate the exact nature of flows in the gas channels.

References

[1] X. Liu, H. Guo, F. Ye, C.F. Ma, Electrochim. Acta (2007) 3607.
[2] G. Shanhai, C.Y. Wang, J. Electrochem. Soc. 154 (2007) 998.
[3] M.M. Mench, C.Y. Wang, M. Ishikawa, J. Electrochem. Soc. 150 (2003) 1052.
[4] G. Maranzana, O. Lottin, T. Colinart, S. Chupin, S. Didierjean, J. Power Sources 180 (2008) 748.
[5] A. Hakenjos, H. Muenter, U. Wittstadt, C. Hebling, J. Power Sources 131 (2004) 213.
[6] A. Su, F.-B. Weng, C.-Y. Hsu, Y.-M. Chen, Int. J. Hydrogen Energy 31 (2006) 1031.

[7] F.-B. Weng, A. Su, C.-Y. Hsu, C.-Y. LeeMickey, J. Power Sources 157 (2006) 674.
[8] T. Ous, C. Arcoumanis, J. Power Sources 173 (2007) 137.
[9] X.G. Yang, F.Y. Zhang, A.L. Lubawy, C.Y. Wang, Electrochem. Solid State Lett. 7 (2004) 408.
[10] C. Hartnig, R. Kuhn, P. Krger, J. Schloesser, I. Manke, Proceedings of the FDFC Nancy, 2008.
[11] J. Bedet, G. Maranzana, S. Leclerc, O. Lottin, C. Moyne, D. Stemmelen, P. Mutzenhardt, D. Canet, Int. J. Hydrogen Energy 33 (2008) 3146.